



Atlantic and Pacific tropics connected by mutually interactive decadal-timescale processes

Gerald A. Meehl¹, Aixue Hu¹, Frederic Castruccio¹, Matthew H. England², Susan C. Bates¹, Gokhan Danabasoglu¹, Shayne McGregor³, Julie M. Arblaster¹, Shang-Ping Xie⁴ and Nan Rosenbloom¹

Decadal climate prediction presumes there are decadal-timescale processes and mechanisms that, if initialized properly in models, potentially provide predictive skill more than one or two years into the future. Candidate mechanisms involve Pacific decadal variability and Atlantic multidecadal variability, elements of which involve slow fluctuations of tropical Pacific and Atlantic sea surface temperatures (SSTs) from positive anomalies (positive phase) to negative anomalies (negative phase). Here we use model experiments to show that there tends to be a weak opposite-sign SST response in the tropical Pacific when observed SSTs are specified in the Atlantic, while there is a weak same-sign SST response in the tropical Atlantic when observed SSTs are specified in the tropical Pacific. Net surface heat flux in the Atlantic and ocean dynamics in the Pacific play contrasting roles in the ocean response to specified SSTs in the respective basins. We propose that processes in the Pacific and Atlantic are sequentially interactive through the atmospheric Walker circulation along with contributions from midlatitude teleconnections for the Atlantic response to the Pacific.

revious studies regarding connections between the Atlantic and Pacific basins often focused on the Walker circulation through the atmosphere, with the Atlantic driving the Pacific¹⁻⁵, the Atlantic driving global decadal variability⁶, the Pacific driving the Atlantic⁷⁻⁹ or the Atlantic affecting the Pacific via the tropical Indian Ocean¹⁰. These influences are typically invoked for the tropics¹¹, although other connections through the midlatitudes have also been proposed^{3,11} with interaction between Pacific and Atlantic decadal variability possibly important for midlatitude teleconnections¹². Two-way interactions between the Atlantic and Pacific have been reviewed for interannual timescales¹¹, and for observations on decadal timescales¹³, although the short data record for the latter did not allow an analysis of the mechanisms involved.

The tropical Atlantic forcing of the tropical Pacific via the anomalous Walker circulation is seen on both interannual and decadal timescales as noted by studies cited in the preceding. However, a major difference on the decadal timescale, which we address in this paper, is that convective heating anomalies in the tropical eastern Pacific, which have been shown to play roles in decadal-timescale Arctic and Antarctic sea ice responses through the Pacific–North American (PNA) and Pacific–South American (PSA) teleconnection patterns, respectively^{14–16}, also end up affecting the tropical North and South Atlantic. Since these processes are acting on decadal timescales, as opposed to the interannual timescale, the responses go beyond single seasons as in the interannual case¹¹. In addition, external forcings play a greater role on the decadal timescales shown here.

Idealized pacemaker experiments

For Pacific decadal variability positive phase (PDV+) minus PDV-, assuming approximate linearity of the interbasin connections, the specified SST pattern in the Pacific (Methods) is characterized by

positive SST anomalies of over $+0.5\,^{\circ}\text{C}$ over most of the tropical Pacific representing the positive PDV phase (Fig. 1a). There are statistically significant positive (same-sign) SST anomalies of several tenths of a degree over most of the tropical Atlantic (Fig. 1a) with significant positive precipitation anomalies that cover most of the Pacific tropics (Fig. 1b, values of around $+0.4\,\text{mm}\,\text{d}^{-1}$). There are mostly positive precipitation anomalies between about 30°N and 30°S in the Atlantic and a narrow band of negative anomalies near 20°S (Fig. 1b) with values of about $\pm 0.2\,\text{mm}\,\text{d}^{-1}$.

For specified positive Atlantic multidecadal variability (AMV+minus AMV-), the tropical Pacific shows opposite-sign (negative) SST anomalies with values of around $-0.2\,^{\circ}$ C (Fig. 1c) that are roughly half the amplitude of the specified PDV pattern in Fig. 1a. Corresponding precipitation anomalies (Fig. 1d) are positive over much of the specified positive SST regions in the tropical Atlantic (values of over about $+0.4\,\mathrm{mm}$ d⁻¹) and negative (around $-0.2\,\mathrm{mm}$ d⁻¹) over most of the tropical Pacific.

The large-scale east—west Walker circulation in the atmosphere connects the basins in the pacemaker experiments with enhanced vertical motion over tropical ocean regions with positive SST anomalies and anomalous descent to the east and west (Fig. 1e,f). Thus, for PDV+ minus PDV-, stronger upward vertical motion over the eastern tropical Pacific is associated with weaker Pacific trade winds (westerly anomaly winds in the lower troposphere), anomalous descent over the tropical Atlantic and Maritime Continent and upper-level outflow away from the enhanced vertical motion in the tropical Pacific (Fig. 1e). Similarly for the AMV+ minus AMV-, enhanced vertical motion over the tropical Atlantic is associated with outflow near 200 hPa to the west (easterly anomaly winds) and anomalous descent over the tropical Pacific with trade-wind acceleration there (easterly anomaly winds in the lower troposphere, Fig. 1f).

¹National Center for Atmospheric Research, Boulder, CO, USA. ²Climate Change Research Centre (CCRC), University of New South Wales, Sydney, New South Wales, Australia. ³ARC Centre of Excellence for Climate Extremes, and School of Earth, Atmosphere and Environment, Monash University, Clayton, Victoria, Australia. ⁴Scripps Institution of Oceanography, La Jolla, CA, USA. [™]e-mail: meehl@ucar.edu

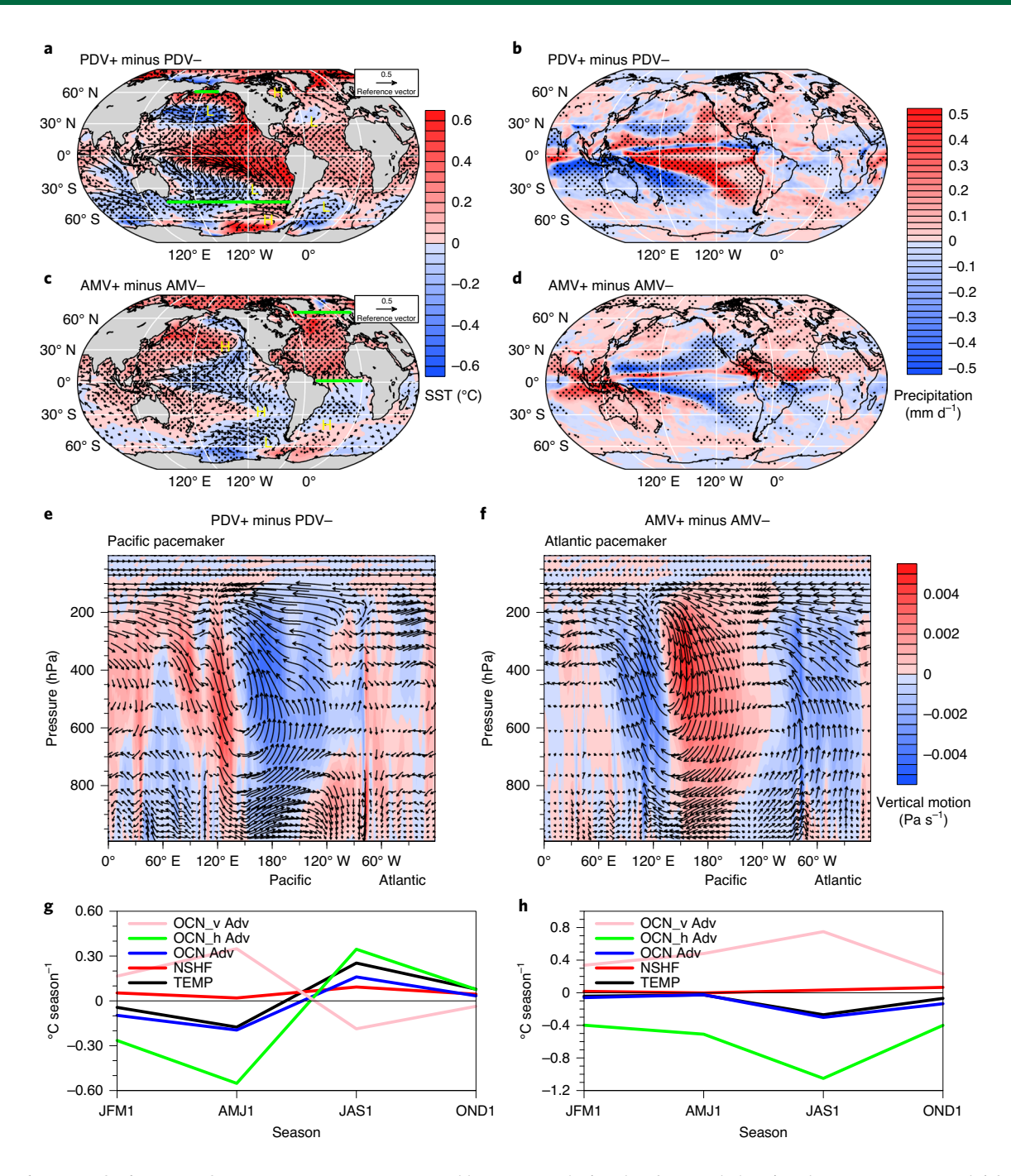


Fig. 1 | Mechanisms of Atlantic-Pacific connections. a, Ten-year ensemble mean SSTs (°C) and surface winds (ms⁻¹, scaling vector in upper right) for PDV+ minus PDV-; 95% significance is stippled; horizontal dark green lines demarcate area of specified Pacific pacemaker SSTs; anomalous cyclonic circulations denoted by 'L' and anticyclonic by 'H' to correspond to sea level pressure anomalies in Supplementary Fig. 4. b, Same as **a** except for precipitation (mm d⁻¹). **c**, Same as **a** except for Atlantic multidecadal variability positive phase (AMV+) minus AMV-; horizontal dark green lines demarcate area of specified Atlantic pacemaker SSTs. **d**, Same as **b** except for AMV+ minus AMV-. **e**, Ten-year ensemble mean cross section of winds averaged from 5° S to 15° N (vectors) and vertical motion (Pa s⁻¹; anomalous upward vertical motion is blue; downward motion is red) for the PDV+ minus PDV- experiment. **f**, Same as **e** except for the AMV+ minus AMV- experiment. **g**, Ocean heat budget for the upper 100 m for the response of the east Atlantic (35° W-10° E, 5° S-5° N) in the PDV pacemaker for seasons in the first year, January-February-March (JFM1), April-May-June (AMJ1), July-August-September (JAS1), and October-November-December (OND1). **h**, Response of the equatorial east Pacific (120° W-180°, 5° S-5° N) in the AMV pacemaker, seasonal trends of net ocean advection (OCN Adv, standard deviation of 0.3 for **g**, 0.4 for **h**), net surface heat flux (NSHF, standard deviation of 0.1 for both **g** and **h**), upper 100 m heat storage (change of temperature with time, dT/dt, labelled TEMP, standard deviation of 0.8 for **g**, 1.8 for **h**), all in °C season⁻¹.

To identify the contributions to seasonal SST anomalies in the Pacific and Atlantic pacemaker experiments (differences calculated for PDV+ minus PDV- and AMV+ minus AMV-), area averages

are computed for the PDV pacemaker experiment over the equatorial Atlantic (35° W–10° E, 5° S–5° N, Fig. 1g) and for the AMV pacemaker for the eastern equatorial Pacific (120° W–180°, 5° S–5° N,

ARTICLES NATURE GEOSCIENCE

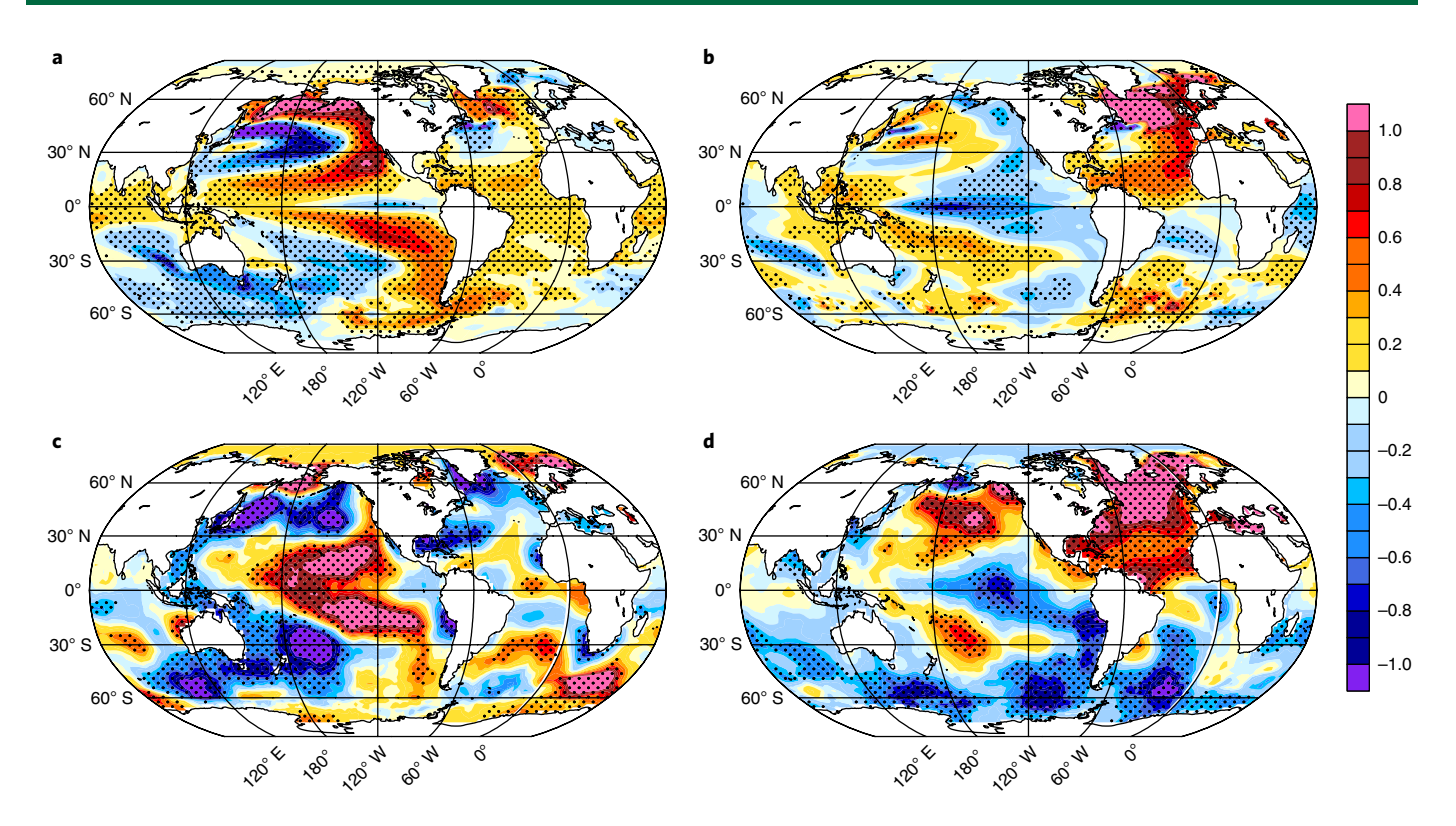


Fig. 2 | Atlantic-Pacific two-way leads/lags. a, Lagged regressions of annual-mean SST on the simulated PDV index from the 1,800-year CESM1 LENS pre-industrial control; PDV leads by three years. **b**, Same as **a** except tropical Atlantic (AMV index) leads by three years. **c**, Regression plots based on observed SSTs from Extended Reconstructed Sea Surface Temperature (ERSST) v.4; PDV leads by three years. **d**, Same as **c** except AMV leads by three years. Units on the colour bar are °C per °C of AMV or PDV. Stippling indicates regions that are significant above the 95% confidence level on the basis of a two-sided *t* test. Supplementary Fig. 5 shows similar patterns for lead years 1–5 for the CESM1, and Supplementary Fig. 6 for the observations.

Fig. 1h). These areas are chosen to capture regions where there is a uniform-sign response of SSTs in each of the pacemaker experiments (Fig. 1a,c). Quantities include upper 100 m heat storage, the total ocean advection contribution to trends in the heat storage in the upper 100 m (a thinner 50 m layer shows similar results) as well as the horizontal and vertical advection contributions and net surface heat flux (Methods).

The response to the PDV+SST anomalies (PDV+ minus PDV-) for the tropical Atlantic box (Fig. 1g) shows small positive net surface heat flux seasonal trend anomalies through all seasons, with the biggest positive contribution from net longwave radiation (Supplementary Fig. 3g). Meanwhile, the initial cooling due to ocean advection, with the largest contributions from horizontal advection, arises from the anomalous Walker circulation spinning up (Fig. 1e) producing stronger easterlies along the Equator (Supplementary Fig. 1a,c). This shifts to a warming tendency by July-August-September (JAS1) as less heat diverges out from the equatorial region due to horizontal advection. Meanwhile, positive precipitation and associated convective heating anomalies in the eastern tropical Pacific (Fig. 1b) are associated with the establishment of a PNA pattern to the north and east and an anomalous PSA pattern to the south and east, each with alternating anomalous low- and high-pressure centres noted in Fig. 1a (and Supplementary Fig. 4a) ending with anomalous low centres in the North and South Atlantic.

There are anomalous westerly component surface winds radiating out from those circulation centres that extend to the tropical North and South Atlantic (Fig. 1a), thus weakening the trade winds north of about 15°N and south of around 15°S. These weakened trades act to reduce latent heat flux in those regions (Supplementary Fig. 3c) and contribute to positive values of net surface heat flux

(Supplementary Fig. 3i), which act to warm the ocean surface. Equatorward of those areas, there are weak southeasterly anomaly surface winds (Fig. 1a) in association with the anomalous Walker circulation being driven from the tropical Pacific (Fig. 1e). By JAS1, that warmer water to the south contributes to horizontal ocean heat convergence (Fig. 1g). With warming due to both weakened horizontal advection and net surface heat flux trends, the net result is enhanced upper-ocean heat storage during JAS1 and OND1 (Fig. 1g) and positive SST anomalies (Supplementary Fig. 1g). As SSTs warm over most of the tropical Atlantic (Fig. 1a,e,g), there is weakly enhanced precipitation (Fig. 1b) and associated increases of low cloud (Supplementary Fig. 3m) that contribute to enhanced downward longwave radiation (Supplementary Fig. 3g). This contributes to the net positive surface heat flux in JAS1 and October-November-December (OND1) (Fig. 1g) that contributes to warming the upper ocean (Fig. 1g). Thus, for the Atlantic response to the Pacific pacemaker, midlatitude contributions from anomalous PNA and PSA circulations that act to weaken the trades and warm the surface combined with the anomalous Walker circulation that maintains anomalous southeasterlies in the equatorial Atlantic (Fig. 1a) contribute to ocean heat convergence that helps warm the surface layer.

By contrast, cooling contributions from ocean advection, dominated by horizontal advection that is diverging heat from the surface layer (Fig. 1h), in association with easterly anomaly surface winds (Fig. 1c) that are a product of the anomalous Walker circulation (Fig. 1f), are dominant in the tropical eastern Pacific in response to AMV + SST anomalies (Fig. 1h). This leads to the development of negative upper-ocean heat-storage anomalies there, with net surface heat fluxes playing only a minor role (Fig. 1h). As noted previously, midlatitude teleconnections play less of a role than the Walker

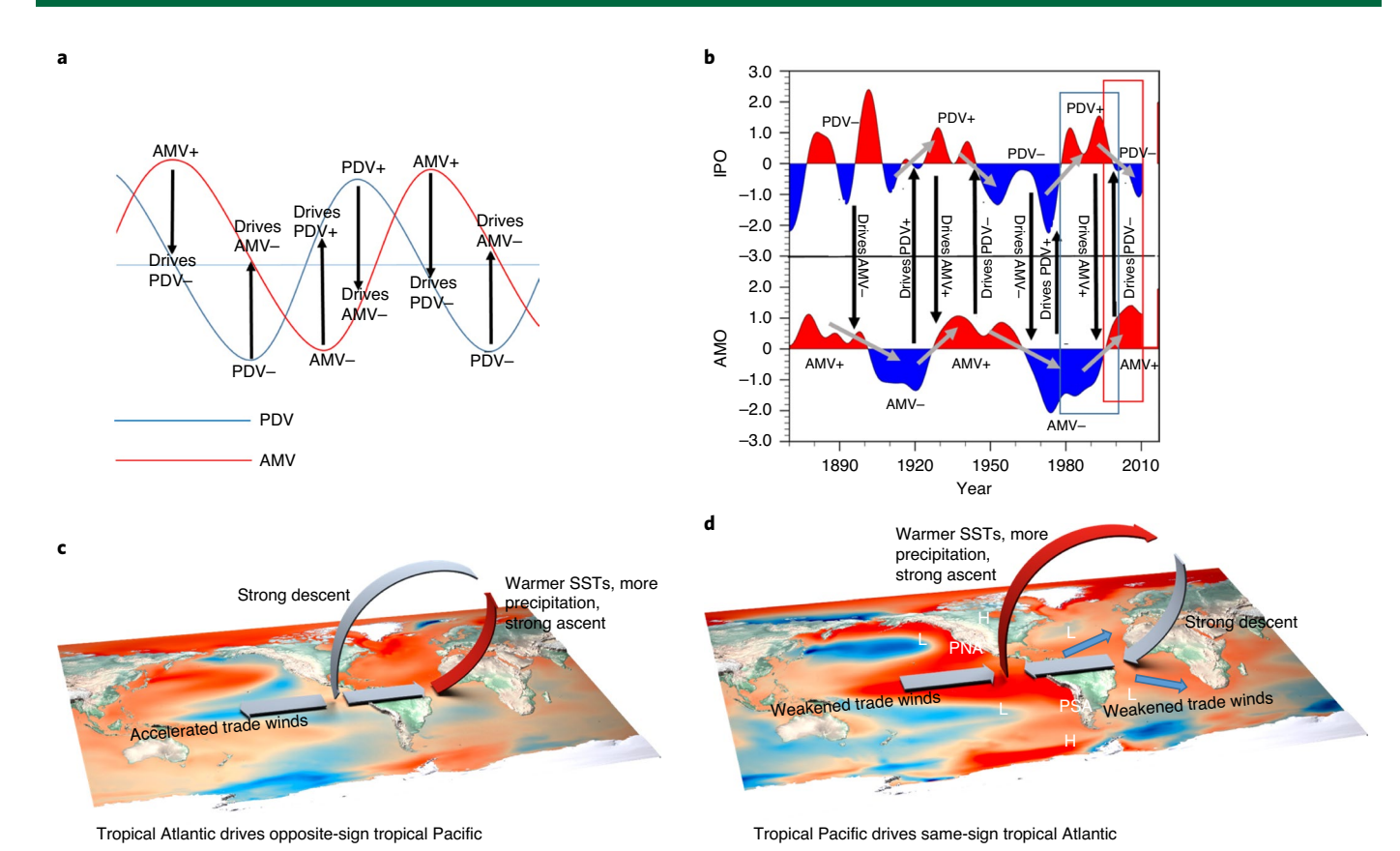


Fig. 3 | Decadal Atlantic-Pacific interactions. a, Idealized schematic of mutual interactions between tropical Atlantic and tropical Pacific. Black arrows indicate direction of influence. The tropical Pacific contributes to making the tropical Atlantic SSTs the same sign, and the Atlantic then contributes to making the tropical Pacific SSTs opposite sign. Although shown in this schematic as oscillatory phenomena, this is an idealized depiction since the PDV and AMV represent 10- to 30-year timescale phenomena as seen in **b**. **b**, Observed time series of PDV (top line) and AMV (bottom line) corresponding to the idealized schematic in **a** and showing that PDV and AMV are not oscillatory but represent 10- to 30-year timescales of variability. Black arrows indicate direction of influence; grey arrows show direction of trends in indices; blue box outlines period in Fig. 4 from 1975 to 2000; red box outlines period in Fig. 5 from 1996 to 2010. **c**, Schematic representation of basin interactions for positive AMV contributing to opposite-sign SST response of negative PDV in the tropical Pacific mainly through the tropical Walker circulation as in, for example, the red-box period in panel **b** (background SST anomalies from the tropical Walker circulation as well as extratropical teleconnections driven by positive precipitation and convective heating anomalies in the tropical Pacific to produce a PNA pattern across North America (sequence of 'L—H—L' indicating wave train of anomalous low-high-low SLP anomalies) and a comparable PSA pattern across South America as in, for example, the blue-box period in panel **b** (background SST anomalies from Fig. 1a).

circulation connections from the tropical Atlantic to the tropical Pacific. As the tropical Pacific cools, there are anomalous anticyclonic circulations in the North and South Pacific (Fig. 1c) associated with positive SLP anomalies there and a weak PSA pattern (Supplementary Fig. 4b). This could be expected as a product of the negative convective heating anomalies associated with the negative precipitation anomalies (Fig. 1d) and not necessarily as being driven directly by the tropical Atlantic.

Horizontal advection plays a dominant role in both tropical basins, but a warming advection tendency in the second half of the first year in the tropical Atlantic, in response to positive SST anomalies in the tropical Pacific in the Pacific idealized pacemaker (Fig. 1a), combines with net surface air–sea heat-flux gains to produce positive anomalies in upper-ocean heat storage (and positive SSTs) by the second half of the first year (Fig. 1g) and a same-sign SST response in the tropical Atlantic and Pacific (Fig. 1a). There are contributions to the anomalous wind forcing in the tropical Atlantic from both the anomalous Walker circulation and midlatitude teleconnections driven by convective heating anomalies in the Pacific. Meanwhile, for the idealized Atlantic pacemaker experiment, ocean advection, driven by the surface easterly wind

anomalies from the anomalous Walker circulation, plays the dominant role in the eastern Pacific in contributing to negative seasonal trends in upper-ocean heat storage as more heat diverges out from the equatorial region due to horizontal advection (Fig. 1h). Midlatitude teleconnections from the tropical Atlantic to the tropical Pacific are not a major factor in the Pacific response in agreement with previous studies. In the end, there is an opposite-sign SST response in the tropical Pacific to the imposed SST forcing in the tropical Atlantic (Fig. 1c).

Atlantic-Pacific two-way connections in observations and a model

The question remains as to whether these kinds of contrasting responses can be seen either in conventional fully coupled model simulations or in observations. To address the first component, using the 1,800-year Community Earth System Model (CESM1) large-ensemble (LENS) pre-industrial control simulation, we perform a lagged regression of the winter (December–January–February–March) SST on simulated AMV and PDV indices (Methods). Consistent with the results from the idealized experiments in the preceding, there is a positive PDV phase

ARTICLES NATURE GEOSCIENCE

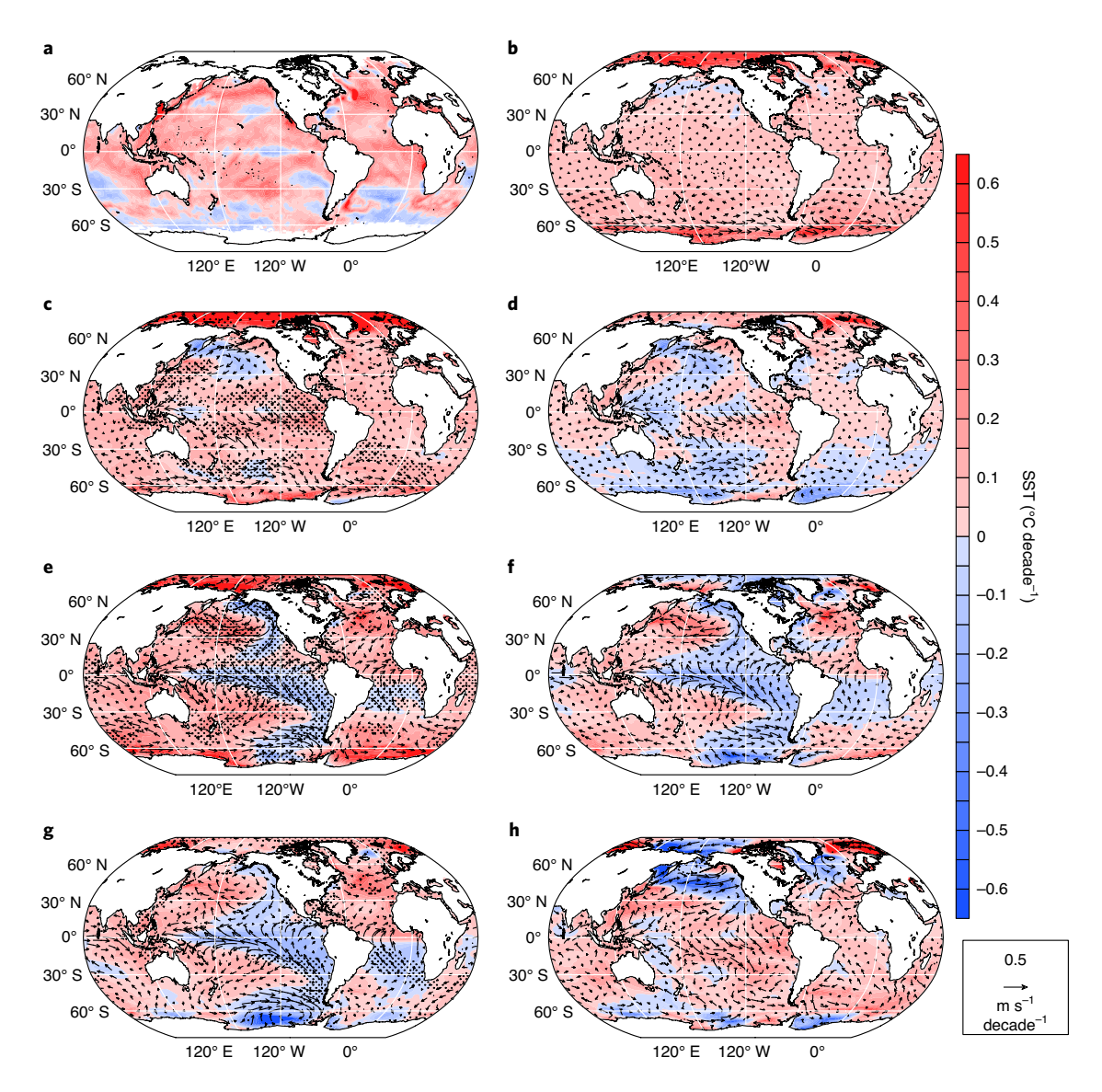


Fig. 4 | Positive PDV and AMV trending positive to negative. SST trend for the time-series pacemakers (Methods) calculated from 1975 to 2000 for positive PDV and AMV trending from negative to positive. **a**, Observed SSTs from Hadley Centre Sea Ice and Sea Surface Temperature (HadISST). **b**, Ensemble average from LENS representing externally forced signal, SST (colours, °C decade⁻¹) and surface winds (vectors, m s⁻¹, scaling arrow at lower right). **c**, Pacific pacemaker ensemble mean (EM). **d**, Pacific pacemaker in **c** minus LENS in **b**. **e**, Atlantic pacemaker EM. **f**, Atlantic pacemaker in **e** minus LENS in **b**. **g**, Atlantic pacemaker. Stippling in left panels for model pacemaker experiments indicates regions that are significant above the 95% confidence level on the basis of a two-sided t test.

when AMV lags by one to five years (or tropical Pacific leads with same sign, Supplementary Fig. 5), with the three-year lag result from Supplementary Fig. 5 shown in Fig. 2a to illustrate this pattern. Conversely, there is a negative PDV phase when AMV leads (opposite sign) for one- to five-year lags (Supplementary Fig. 5) with the result for the three-year lag shown in Fig. 2b as an example of this pattern. In the first season of the idealized pacemaker experiments, there is already a notable influence from one basin to the other (discussed in relation to Fig. 1g,h, and Supplementary Figs. 1 and 2) that is present in the decadal averages (Fig. 1a,c). Thus, these signals are already visible at lead and lag one year in Supplementary Fig. 5. Relative amplitudes of the patterns for different lags in Supplementary Fig. 5 are instructive but not definitive (as in Supplementary Fig. 6 for the observations from a much shorter period) since similar signs present in the patterns are comparable to the idealized pacemakers. This reinforces the idea that the tropical

Atlantic and Pacific basins influence each other differently depending on which is leading the other during different periods.

The interpretation of a similar lag regression calculation from observations is less straightforward due to the short record length and the complicating role of external forcings^{17–19}. Nevertheless, lag regressions from the observations calculated for the tropical Pacific leading by one to five years (Supplementary Fig. 6) show a similar pattern at all leads as illustrated by the three-year lead in Fig. 2c (a same-sign response in most of tropical Atlantic just north of the Equator, although there are negative anomalies in the North Atlantic that were not present in the model control run, Fig. 2a). For the example of the tropical Atlantic leading by one to five years (Supplementary Fig. 6), there are also similar patterns at all leads as illustrated by the three-year lead where there is an opposite-sign response in most of the tropical Pacific (Fig. 2d), similar to the idealized Atlantic pacemaker (Fig. 1c) and the long model control

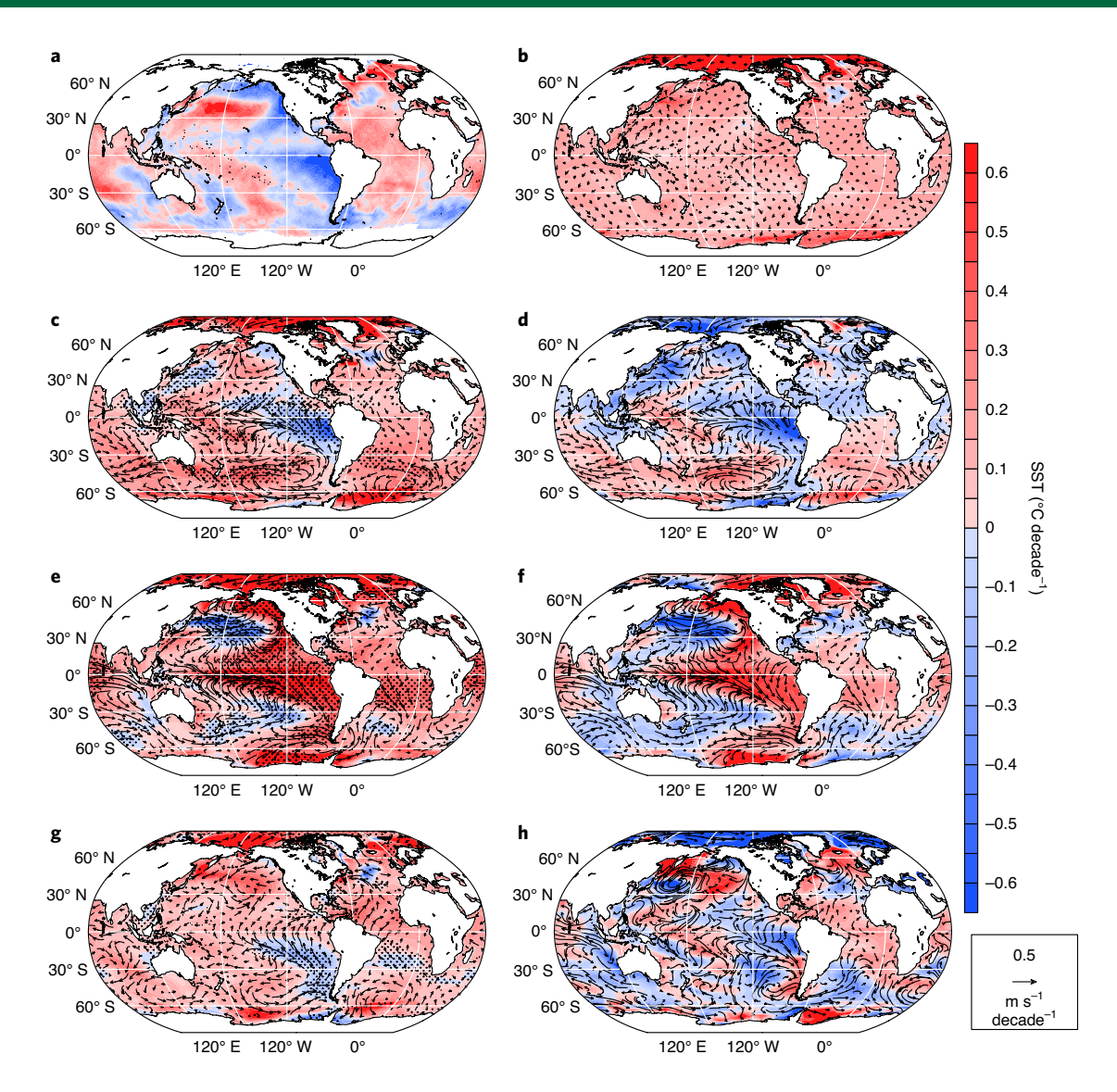


Fig. 5 | Positive AMV and PDV trending positive to negative. SST trend for the time-series pacemakers (Methods) calculated from 1996 to 2010 for positive AMV and PDV trending from positive to negative. **a**, Observed SSTs from HadISST. **b**, Ensemble average from LENS representing externally forced signal, SST (colours, °C decade⁻¹) and surface winds (vectors, ms⁻¹, scaling arrow at lower right). **c**, Pacific pacemaker EM. **d**, Pacific pacemaker in **c** minus LENS in **b**. **e**, Atlantic pacemaker EM. **f**, Atlantic pacemaker in **e** minus LENS in **b**. **g**, Atlantic pacemaker EM with aerosols fixed at 1920 values. **h**, Same as **g** except for Pacific pacemaker. Stippling in left panels for model pacemaker experiments indicates regions that are significant above the 95% confidence level on the basis of a two-sided *t* test.

simulation (Fig. 2b). As shown in Fig. 1g,h, fast processes in the atmosphere force a response in the ocean that sets up in the first year of the experiment. These anomalies are then sustained for leads of up to five years. This provides further evidence that the tropical Pacific and tropical Atlantic are mutually interactive, suggesting that each basin alternately contributes to a response in the other.

Illustrations of decadal Atlantic-Pacific interactions

A simplified schematic illustration of these interactions (Fig. 3a) shows how positive AMV could contribute to an opposite-sign trend to negative PDV and negative PDV could then contribute to a same-sign trend from positive to negative AMV. The converse could then be the case for negative AMV contributing to a trend from negative to positive PDV (opposite sign) and then that positive PDV phase contributing to a trend from negative to positive AMV (same sign). This schematic illustration is in no way intended to depict actual time series or to imply that either PDV or AMV is an oscillatory phenomenon. AMV and PDV are characterized by timescales

of variability from about 10 to 30 years and are not oscillatory²⁰. In our interpretation of the pacemaker experiments, each basin can influence the other on these timescales but not drive an oscillation.

PDV and AMV indices derived from observations (Fig. 3b and Methods) show how the positive and negative PDV and AMV states can mutually influence each other (heavy black arrows showing the direction of the influence). For example, positive PDV in the 1980s and 1990s could be influencing a trend from negative AMV to positive AMV (arriving at same-sign tropical Pacific and Atlantic, shown schematically in Fig. 3d), and positive AMV in the early 2000s could contribute to a trend from positive to negative PDV (ending up with opposite-sign SST anomalies in the tropical Pacific and Atlantic, Fig. 3c).

Time-series pacemaker experiments

To examine the effects of external forcings in the ocean basin interactions, Figs. 4 and 5 show ensemble average (ten member) results from the time-series pacemaker configurations (Methods). Two

ARTICLES NATURE GEOSCIENCE

periods are shown to follow the example discussed in Fig. 3b,c,d for trends from 1975 to 2000 (roughly positive PDV contributing to a trend to same-sign positive AMV, Figs. 3b,d and 4) and from 1996 to 2010 (positive AMV contributing to a trend to opposite-sign negative PDV, Figs. 3b,c and 5). These are selected to be illustrative, and since the data are low-pass filtered, the results are not sensitive to the exact start and end years of these periods. The Pacific pacemaker in Fig. 4c shows a similar same-sign pattern in the tropical Atlantic seen in the observations (Fig. 4a), with values about +0.1 °C decade⁻¹. Subtracting out the effects of external forcings over this period as represented by the LENS mean (Fig. 4b and Methods) shows a weakened but still same-sign response of mostly positive SST trends in the tropical Atlantic of up to about +0.1 °C decade⁻¹ (Fig. 4d) that retain the sense of the observations (Fig. 4a). For the Atlantic pacemaker (Fig. 4e), there is an opposite-sign response in the tropical Pacific that is consistent with the tropical Atlantic contributing to an opposite-sign response in the Pacific (Fig. 1c) but is not consistent with observations (Fig. 4a) and is similar when the effects of external forcing are removed (Fig. 4f). This indicates that, for this period for this model, the tropical Pacific was probably contributing to the same-sign SST anomalies in the tropical Atlantic.

In the Atlantic pacemaker experiment where the effects of aerosols are removed by fixing aerosols at 1920 values, there is still an opposite-sign response with even greater cooling in the tropical Pacific (Fig. 4g) that is not seen in observations (Fig. 4a). A Pacific pacemaker with aerosols fixed at 1920 values (single member) shows warming trends for this period in the tropical Atlantic (Fig. 4h) and an aerosol-only warming in the tropical North Atlantic as well (Supplementary Fig. 7c). Therefore, some of the tropical North Atlantic response could be forced by aerosols in addition to forcing from the internal SST variability in the Pacific.

The observed trend from 1996 to 2010 shows an opposite-sign SST trend pattern in the tropical Atlantic and Pacific (Fig. 5a). The Pacific pacemaker resembles this pattern (Fig. 5c) but turns into a same-sign negative SST anomaly trend in the tropical Pacific and Atlantic north of the Equator when external forcings are removed (Fig. 5d). For the Atlantic pacemaker, there also is a same-sign response in the two tropical basins (Fig. 5e) even with external forcings removed (Fig. 5f). However, when just aerosols are removed, there is a low-amplitude opposite-sign response between tropical Atlantic and Pacific (Fig. 5g, single member). Since the signature of aerosols only for this period is a weak warming in the tropical eastern Pacific (Supplementary Fig. 7d), the Atlantic pacemaker same-sign response (Fig. 5e) is probably receiving contributions from model-dependent aerosol forcing. When the aerosol effect is removed in Fig. 5g, the opposite-sign response emerges in the tropical Pacific that is qualitatively closer to observations (Fig. 5a). This probably characterizes the opposite-sign negative SST trend response in the Pacific to the positive SST trend in the tropical Atlantic.

Online content

Any methods, additional references, Nature Research reporting summaries, source data, extended data, supplementary information, acknowledgements, peer review information; details of author contributions and competing interests; and statements of

data and code availability are available at https://doi.org/10.1038/s41561-020-00669-x.

Received: 19 November 2019; Accepted: 10 November 2020; Published online: 14 December 2020

References

- McGregor, S. et al. Recent Walker circulation strengthening and Pacific cooling amplified by Atlantic warming. *Nat. Clim. Change* https://doi. org/10.1038/NCLIMATE2330 (2014).
- McGregor, S. et al. Model tropical Atlantic biases underpin diminished Pacific decadal variability. Nat. Clim. Change https://doi.org/10.1038/s41558-018-0163-4 (2018).
- Ruprich-Robert, Y. et al. Assessing the climate impacts of the observed Atlantic multidecadal variability using the GFDL CM2.1 and NCAR CESM1 global coupled models. J. Clim. 30, 2785–2810 (2017).
- Levine, A. F. Z., McPhaden, M. J. & Frierson, D. M. W. The impact of the AMV on multidecadal ENSO variability. *Geophys. Res. Lett.* 44, 3877–3886 (2017)
- Geng, X., Zhang, W. & Jin, F.-F. Modulation of the relationship between ENSO and its combination mode by the Atlantic multidecdal oscillation. *J. Clim.* 33, 4679–4695 (2020).
- Yang, Y.-M., An, S.-I., Wang, B. & Park, J. H. A global-scale multidecadal variability driven by Atlantic multidecadal oscillation. *Natl Sci. Rev.* 7, 1190–1197 (2020).
- Kumar, A., Bhaskar, J. & Wang, H. Attribution of SST variability in global oceans and the role of ENSO. Clim. Dyn. 43, 209–220 (2014).
- Taschetto, A. S., Rodrigues, R. R., Meehl, G. A., McGregor, S. & England, M. H. How sensitive are the Pacific–North Atlantic teleconnections to the position and intensity of El Niño-related warming. *Clim. Dyn.* https://doi. org/10.1007/s00382-015-2679-x (2015).
- Meehl, G. A., Hu, A., Santer, B. D. & Xie, S.-P. Contribution of the Interdecadal Pacific Oscillation to twentieth-century global surface temperature trends. Nat. Clim. Change https://doi.org/10.1038/nclimate3107 (2016).
- Li, X., Xie, S.-P., Gille, S. T. & Yoo, C. Atlantic-induced pan-tropical climate change over the past three decades. *Nat. Clim. Change* https://doi. org/10.1038/NCLIMATE2840 (2015).
- 11. Cai, W. et al. Pantropical climate interactions. Science 363, eaav4236 (2019).
- 12. Elsbury, D. et al. The atmospheric response to positive IPV, positive AMV, and their combination in boreal winter. *J. Clim.* **32**, 4193–4213 (2019).
- 13. Nigam, S., Sengupta, A. & Ruiz-Barradas, A. Atlantic-Pacific links in observed multidecadal SST variability: is the Atlantic multidecadal oscillation's phase reversal orchestrated by the Pacific decadal oscillation? *J. Clim.* **33**, 5479–5505 (2020).
- Meehl, G. A., Chung, C. T. Y., Arblaster, J. M., Holland, M. M. & Bitz, C. M. Tropical decadal variability and the rate of Arctic sea ice retreat. *Geophys. Res. Lett.* https://doi.org/10.1029/2018GL079989 (2018).
- Meehl, G. A., Arblaster, J. M., Bitz, C., Chung, C. T. Y. & Teng, H. Antarctic sea ice expansion between 2000–2014 driven by tropical Pacific decadal climate variability. *Nat. Geosci.* https://doi.org/10.1038/NGEO2751 (2016).
- Meehl, G. A. et al. Sustained ocean changes contributed to sudden Antarctic sea ice retreat in late 2016. Nat. Commun. 10, 14 (2019).
- Booth, B. B. B., Dunstone, N. J., Halloran, P. R., Andrews, T. & Bellouin, N. Aerosols implicated as a prime driver of twentieth-century North Atlantic climate variability. *Nature* 484, 228–232 (2012).
- Smith, D. M. et al. Role of volcanic and anthropogenic aerosols in the recent global surface warming slowdown. *Nat. Clim. Change* https://doi.org/10.1038/ NCLIMATE3058 (2016).
- Watanabe, M. & Tatebe, H. Reconciling roles of sulphate aerosol forcing and internal variability in Atlantic multidecadal climate changes. *Clim. Dyn.* 53, 4651–4665 (2019).
- Cassou, C. et al. Decadal climate variability and predictability. Bull. Am. Meteorol. Soc. https://doi.org/10.1175/BAMS-D-16-0286.1 (2018).

Publisher's note Springer Nature remains neutral with regard to jurisdictional claims in published maps and institutional affiliations.

 $\ensuremath{\texttt{©}}$ The Author(s), under exclusive licence to Springer Nature Limited 2020

Methods

The global coupled climate model version used here is the CESM1-CAM5 model (hereafter, CESM1) that is the same model described in the CESM LENS Project 21 . All components have approximately $1^{\rm o}$ horizontal resolution. The ocean has 60 levels in the vertical and a meridional mesh refinement down to a quarter of a degree near the Equator, while the atmospheric component has 30 hybrid vertical levels.

To create the idealized patterns to which the model is restored³, the internal component of the observed Pacific and Atlantic decadal-timescale variability is separated from the externally forced part²². To first estimate the externally forced part, signal-to-noise maximizing empirical orthogonal functions (EOFs) are applied to the Coupled Model Intercomparison Project Phase 5 multimodel ensemble with historical and representative concentration pathway 8.5 (RCP 8.5) simulations for the 1870-2005 and the 2006-2013 periods, respectively. This produces an estimate of the time series of the radiatively forced component of SST as PC1 of the global signal-to-noise EOF, and the spatial pattern is derived by regressing the observed global SST (ERSSTv.323) onto the PC1 time series. The internally generated SST components are then obtained as the residuals of the observed North Atlantic and Pacific SSTs (resembling the AMV and PDV) for Equator to 60° N, 75° W to 7.5° W, and 40°S to 60°N, respectively, after subtracting the externally forced component. The AMV and PDV spatial patterns of SST are then calculated by regressing the residuals of the annual-mean observed SST time series obtained as described in the preceding onto the respective AMV and PDV indices (for more on how indices are defined, see discussion that follows). These index time series and the SST fields are low-pass filtered for the period 1870-2013 before the regressions using a Lanczos filter with a ten-year cut-off period using 21 weights.

Two sets of 30-member ensemble simulations are run for the idealized specified PDV and AMV configurations. The simulations for the AMV configuration are a subset of those used in ref. ³. All external forcings are held constant at pre-industrial values. One set consists of simulations for AMV+ and AMV-; the other set has the simulations for PDV+ and PDV-. Each experiment is run for ten years during which the respective specified seasonal cycle of SST anomalies in the respective areas are kept constant in time while the rest of the model is fully coupled. The 30 ensemble members for each experiment are formed by introducing round-off perturbations in the initial atmospheric temperature.

We use 20 ensemble members randomly selected from the CESM LENS²¹. All ensemble members follow the same radiative-forcing scenario (anthropogenic and natural historical forcings for 1920–2005 and RCP 8.5 forcings from 2006 onwards). As with the idealized simulations, this ensemble is also created by introducing a slight perturbation of the initial atmospheric temperature²¹.

The time-series pacemakers follow the methodology of ref. 24 and include time-evolving external forcing as in the LENS. The Pacific pacemakers in Figs. 4 and 5 nudge the time-evolving SSTs towards observed values over 15° S- 15° N, 180° to the American coast with time-varying external forcings as in the LENS. The rest of the model is fully coupled. Ten ensemble members were run for the period $1920-2013^{25}$. For the Atlantic pacemakers in Figs. 4 and 5, the SSTs are nudged over the area from the Equator to 60° N over the width of the Atlantic basin at those latitudes.

The SST nudging for the Atlantic and Pacific time-series pacemaker experiments is performed by computing the sensible heat flux from the observational SST anomalies that have been added to the model climatology and applying that to the coupled model. Observed SSTs are those from the National Oceanic and Atmospheric Administration ERSSTv.3b dataset. Between 15°S and 20°S and between 15°N and 20°N in the Pacific, and from the Equator to 5°S in the Atlantic, buffer belts were created with nudged SST tapering to the fully coupled SSTs using linear interpolation as the model runs²⁵. The fixed-aerosol Atlantic and Pacific pacemaker experiments employ the same procedure as the time-series pacemakers but hold the global pattern of anthropogenic aerosol concentrations fixed at their 1920 values with a single ensemble member, while the rest of the external forcings evolve as in the LENS.

The AMV and PDV indices are the observed SSTs from ERSSTv.4 detrended by removing the global SST average 56 then computing a North Atlantic (7.5° W–75° W, 0°–60° N) and tropical Pacific (150° E–90° W, 20° N–20° S) index, with a low-pass Butterworth filter with a ten-year cut-off applied to the time series. For the model, the same procedure is applied without detrending because the time series is from a long control run with little trend. For the purposes of the schematic depiction of the AMV and PDV in Fig. 3, the indices are the deviation from the linearly detrended climatological mean for the spatially averaged North Atlantic SST, Equator–65° N, 0°–85° W. A low-pass Lanczos filter with a 13-year cut-off is applied to the time series. The PDV index is the first EOF of the linearly detrended 13-year Lanczos low-pass filtered SSTs in the Pacific basin. This method produces a somewhat different amplitude time series but with similar zero crossings as in the Trenberth and Shea method 36 to illustrate the cross-basin connections in the schematic.

The results in Fig. 1g,h for the ocean heat budget are calculated by:

$$H_{\rm tot} = {\rm NSHF} + H_{\rm ocean} \tag{1}$$

where

$$H_{\text{ocean}} = H_{\text{o_advection}} + H_{\text{diff}} + H_{\text{submeso}} + H_{\text{mixing}}$$
 (2)

 $H_{o_advection} = OCN_v Adv + OCN_h Adv$ (3)

 $H_{\rm tot}$ in Equation (1) is the total net temperature change (or heat storage) of the upper 100 m layer (°C season $^{-1}$) averaged over the two ocean areas. These areas were chosen on the basis of the regions of largest change of SST in the first four seasons of the idealized pacemaker simulations shown in Supplementary Figs. 1 and 2. The terms on the right of Equation (1) are net surface heat flux (NSHF) and net ocean heat transport ($H_{\rm ocean}$); $H_{\rm ocean}$ is calculated from the different terms making up the heat transport due to the effects of advection ($H_{\rm o,advection}$), diffusion ($H_{\rm diff}$), submesoscale processes ($H_{\rm submeso}$) and mixing due to K-profile parameterization (KPP) and diabatic processes over the upper 100 m ($H_{\rm mixing}$). Here we show the largest terms in the budget for these regions in Equation (3) for $H_{\rm o,advection}$ as horizontal ocean advection, OCN_h Adv, and vertical ocean advection, OCN_v Adv.

Data availability

HadISST data are available from https://www.metoffice.gov.uk/hadobs/hadisst/. The ERA-I data are available from https://www.ecmwf.int/en/forecasts/datasets/reanalysis-datasets/era-interim. ERSSTv4 data are available from https://www.ncdc.noaa.gov/data-access/marineocean-data/extended-reconstructed-sea-surface-temperature-ersst-v4.

Code availability

Previous and current CESM versions are freely available at www.cesm.ucar.edu:/models/cesm2/. The CESM solutions/datasets used in this study are also freely available from the NCAR Digital Asset Services Hub (DASH) at data.ucar.edu or from the links provided from the CESM website at www.cesm.ucar.edu.

References

- Kay, J. E. et al. The Community Earth System Model (CESM) large ensemble project: a community resource for studying climate change in the presence of internal climate variability. *Bull. Am. Meteorol. Soc.* 96, 1333–1349 (2015).
- 22. Ting, M., Kushnir, Y., Seager, R. & Li, C. Forced and internal twentieth-century SST trends in the North Atlantic. *J. Clim.* 22, 1469–1481 (2009).
- Smith, T. M., Reynolds, R. W., Peterson, T. C. & Lawrimore, J. Improvements to NOAA's historical merged land-ocean surface temperature analysis (1880–2006). J. Clim. 21, 2283–2296 (2008).
- Kosaka, Y. & Xie, S.-P. Recent global-warming hiatus tied to equatorial Pacific surface cooling. *Nature* 501, 403–407 (2013).
- Schneider, D. P. & Deser, C. Tropically driven and externally forced patterns of Antarctic sea ice change: reconciling observed and modeled trends. Clim. Dyn. https://doi.org/10.1007/s00382-017-3893-5 (2017).
- Trenberth, K. E. & Shea, D. R. Atlantic hurricanes and natural variability in 2005. Geophys. Res. Lett. https://doi.org/10.1029/2006GL026894 (2006).

Acknowledgements

Portions of this study were supported by the Regional and Global Model Analysis (RGMA) component of the Earth and Environmental System Modeling Program of the US Department of Energy's Office of Biological & Environmental Research (BER) via National Science Foundation IA 1947282. This work also was supported by the National Center for Atmospheric Research, which is a major facility sponsored by the National Science Foundation (NSF) under Cooperative Agreement No. 1852977. F.C. was supported by the NSF under the Collaborative Research EaSM2 Grant OCE-1243015 and EaSM3 Grant OCE-1419569 and by the NOAA Climate Program Office under the Climate Variability and Predictability Program Grant NA13OAR4310138. J.M.A., M.H.E. and S.M. were supported by the Australian Research Council through grant CE110001028, while S.M. was also supported by the Australian Research Council through grant FT160100162. Computing resources (https://doi.org/10.5065/DGRX99HX) were provided by the Climate Simulation Laboratory at NCAR's Computational and Information Systems Laboratory, sponsored by the National Science Foundation and other agencies.

Author contributions

G.A.M. directed this work with contributions from all authors. G.A.M., A.H. and F.C. performed the analyses. All of the authors discussed the results and contributed to writing the manuscript.

Competing interests

The authors declare no competing interests.

Additional information

Supplementary information is available for this paper at https://doi.org/10.1038/s41561-020-00669-x.

Correspondence and requests for materials should be addressed to G.A.M.

Peer review information Primary Handling Editor: James Super. *Nature Geoscience* thanks Mingfang Ting, Yu Kosaka and the other, anonymous, reviewer(s) for their contribution to the peer review of this work.

Reprints and permissions information is available at www.nature.com/reprints.